Arabian Journal of Geosciences (2021) 14: 1279
https://doi.org/10.1007/s12517-021-07548-8

ORIGINAL PAPER

Mineralogy and geochemistry of calc-alkaline magmatic rocks from the Mansehra Granitic Complex, NW Himalaya, Pakistan: insights into petrogenesis and tectonic setting

Mustansar Naeem[1] · Tehseen Zafar[1,2] · Muhammad Nawaz Chaudhry[3] · Jean-Pierre Burg[4] · Nasir Ahmad[1] · Hafiz Ur Rehman[5]

Received: 2 February 2021 / Accepted: 7 June 2021 / Published online: 29 June 2021

Abstract

The Mansehra Granitic Complex (MGC) is mainly comprised of Mansehra Granite, Hakale Granite, pegmatitic, microgranitic, and leucogranitic bodies in the northwest Lesser Himalaya of Pakistan. The Mansehra Granite is generally massive but occasionally gneissic due to local shearing manifested by solid-state deformation. Geochemical classification diagrams placed these plutonic rocks in calc-alkaline, peraluminous granite fields. The zircon saturation temperatures of the Mansehra Granite, Hakale Granite, and Leucogranite are 749–852, 709–779, and 749–754 °C, respectively. The temperature range (709–852 °C) of the MGC rocks is comparable with crystallization temperatures (670–817 °C) of the peraluminous S-type Lesser Himalayan Indian granites. Rb/Sr and Sr/Ba ratios suggest that the granitic melt of Mansehra Granite was derived through biotite dehydration-melting of the protolith Tanawal Formation at > 5 kbr pressure and > 700 °C temperature, whereas the Hakale Granite magma was generated at a relatively shallower depth and lower temperatures by muscovite fluid-absent anatexis of the source rock. The occurrence of andalusite in the contact aureole of Mansehra Granite, presence of perthitic microcline along with negative Nb, Sr, and Ti anomalies in spider diagram and higher Rb/Sr ratios reveal upper crustal signatures and low-pressure shallow emplacement (< 15 km) of the MGC magmatic bodies. The occurrence of psammitic restites, migmatites, and geochemical characteristics suggests the S-type trait of these plutonic rocks. The leucogranitic bodies most likely are the products of Na_2O-rich residual melt and boron-rich fluids of the MGC magma. Harker's variation diagrams indicate that the MG, HG, and LG display significant to poor relationships which suggest imperfect mixing of the non-homogenous protolith during partial crustal melting. However, scattering in some of the plots reflects the heterogeneity of the protolith and irregular distribution of minerals in the granitic melt of the MGC. Owing to affiliation with the continental-continental, syn-collisional geotectonic field, petrogenesis of the MGC rocks can be attributed to an Andean-type Cambro-Ordovician episode along the northern margin of east Gondwana.

Keywords Lesser Himalaya · Zircon saturation thermometry · Biotite dehydration-melting · Geochemical classification · Variations diagrams · Andean-type Cambro-Ordovician episode · Gondwana

Responsible Editor: Domenico M. Doronzo

✉ Tehseen Zafar
zafar@vip.gyig.ac.cn

[1] Institute of Geology, University of the Punjab, Quaid-e-Azam Campus, Lahore 54590, Pakistan

[2] Institute of Geochemistry, Chinese Academy of Sciences, Guiyang 550081, China

[3] College of Earth and Environmental Sciences, University of the Punjab, Quaid-e-Azam Campus, Lahore 54590, Pakistan

[4] Geological Institute, Department of Earth Science, ETH, 8092 Zurich, Switzerland

[5] Department of Earth and Environmental Sciences, Kagoshima University, Kagoshima 890-0065, Japan

Introduction

The Mansehra Granitic Complex (MGC) lies in the Lesser Himalayan Granite Belt in the northwest Himalayas of Pakistan (Fig. 1). The MGC mainly consists of Mansehra Granite (MG), Hakale Granite (HG), and their associated pegmatitic, leucogranitic (LG), and microgranitic bodies (MIG). Geological history, geochemical characteristics, and petrological aspects of this complex were described three decades ago with conventional analytical techniques (e.g., Shams 1971; Ashraf 1992; Best 2003; Singh and Jain 2003; Ogasawara et al. 2019). However, petrogenesis of this complex was limited to theoretical considerations lacking systematic geochemical data. Ogasawara et al. (2019) suggested that the Mansehra Granite was originated by the Late Neoproterozoic to Cambrian sedimentary protoliths. Whereas, Ashraf (1992) proposed that the granite was formed due to partial melting of the pre-existing metamorphic rocks of the area without providing credible evidence in favour of his hypothesis. Naeem et al. (2016) focused mainly on the geochronological investigation of the MGC magmatic rocks and presented limited geochemical studies on petrological aspects of this complex that need to be elaborated through systematic geochemical characterization. Zafar et al. (2019) have shown that Mansehra Granite contains restites of variable size and composition having a similar composition with enclosing sediments of the Tanawal Formation and suggested S-type trait of the granite. However, research work on the geochemical characterization of MGC plutonic rocks is lacking therefore, necessary to shed light on the petrogenesis of the MGC magmatic bodies. The crystallization temperature of a granitic melt plays an important role to find out the mechanism of magma generation. The crystallization temperatures of the Mansehra Granite were estimated by using two-feldspar geothermometry (Shams and Rehman 1967). These temperatures were not used to explain the petrogenesis of the granite. Zircon saturation technique was used in the current study to estimate crystallization temperatures of the MGC rocks. Major and trace elements data was used to determine crystallization temperatures, mechanism of magma generation, and emplacement history of these rocks.

The contradictory hypothesis regarding the origin of the MGC magmatic rocks and lack of systematic investigation necessitates revisiting these plutonic rocks for geochemical characterization and petrogenesis of this complex. The current study presents a systematic geochemical investigation of the MGC plutonic rocks for the petrogenesis of these rocks and the consequent impact on the tectonic settings of the region.

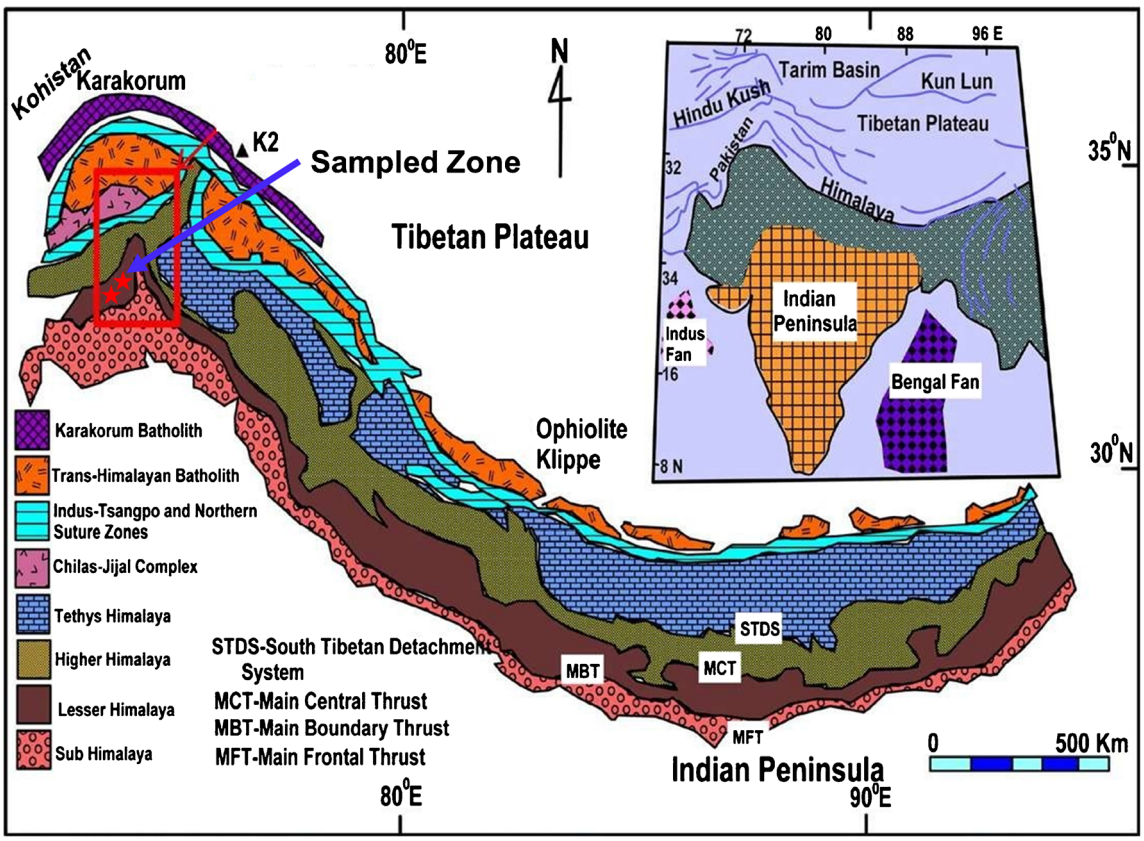

Fig. 1 Map displays the location of the Mansehra area and the main tectonic subdivision of Himalaya. Stars indicate the zone of sampling (Zafar et al. 2019)

Geology of the area

The Himalayan mountain range resulted from a collision between the Indian and Eurasian plates, has been subdivided into four major tectonic elements from north to south into Sub-Himalaya, Lesser Himalaya, Higher, and Tethys Himalaya (Hodges 2000). The Lesser Himalaya is demarcated by the Main Boundary Thrust (MBT) in the south whereas delineated by Main Central Thrust (MCT) in the north. In the Mansehra area, the Lesser Himalaya contains igneous and metamorphic bodies forming the Mansehra Granitic Complex (MGC) which is enclosed by metasediments of the Tanawal Formation, composed of pelite, psammite, phyllite, schists, and quartzite (Fig. 1). The MGC is mainly comprised of Mansehra Granite, Hakale Granite, leucogranites, and microgranites in the Mansehra area (Naeem et al. 2016).

The Mansehra Granite is a two-mica, high potash, medium to coarse-grained porphyritic plutonic body that is generally massive in Oghi-Darband, Phulra, Shagian (KKH), Attar Shisha, Batrasi, and Garhwal area (Naeem 2013). However, due to ductile deformation, local shear zones are developed in the massive Mansehra Granite in Susalgali, Darband, and Jhargali (Fig. 1), where the granite acquires gneissic texture which is manifested by stretched or augen-shaped K-feldspar phenocrysts and deformed quartz wrapped by mica (Fig. 2a; Naeem 2013). The Mansehra Granite intrudes metasediments of the Tanawal Formation. The granite contains restites of variable shapes and sizes which are uniformly dispersed possessing similar composition to the enclosing rocks of the Tanawal Formation (Zafar et al. 2019). U-Pb zircon age of ca. 483–476 Ma has been assigned of the MG (Ogasawara et al. 2019).

The Hakale Granite is a relatively small oval-shaped body that contains tourmaline as a ubiquitous mineral. In Maswal and Pano Dheri, the granite is leucocratic, massive, medium-grained, and poorly to nonporphyritic (Naeem 2013). Based on the LA-ICP-MS zircon U-Pb method, the age of the Hakale Granite is ca. 466 Ma as compared with ca. 483–476 Ma age of the Mansehra Granite (Naeem et al. 2016; Ogasawara et al. 2019). Relatively small microgranitic bodies intrude the metasediments of the Tanawal Formation and Mansehra Granite in Phulra-Bharaina. The microgranites are fine-grained, devoid of K-feldspar phenocrysts, and contain mainly muscovite and tourmaline. In Oghi-Darband and Maswal the microgranites are characterized by parallel to subparallel felsic and tourmaline-bearing layers (Naeem 2013). The leucogranitic bodies occasionally show gneissic fabric as parallel to the subparallel alignment of deformed quartz and augen-shaped K-feldspar phenocrysts (Naeem 2013). U-Pb zircon age of the leucogranitic bodies is ca. 475 Ma (Naeem et al. 2016).

The Tanawal Formation occurs mainly as a pelite-psammite sequence in the Mansehra area. It is composed of pelitic schists of chlorite to kyanite grade with subordinate micaceous quartzite. Andalusite and sillimanite hornfelses as well as injection migmatites occur in the contact aureole of the Mansehra Granite. Sediments of the Tanawal Formation have been metamorphosed from sillimanite to kyanite grades. The metamorphic grade increases from south to north which is not controlled by the intrusion of Mansehra Granite (Naeem 2013). Apophyses of the Mansehra Granite and aplites are commonly found in the metasediments of the Tanawal Formation at the contact (Fig. 2c). In Khaki, the contact is characterized by minor intrusions of the granite having relatively smaller K-feldspar phenocrysts (Fig. 2c–d). Near the contact, migmatites are found as anastomosing layers manifesting intrusion of the granite into the psammitic bands of the Tanawal Formation (Fig. 2e). Banded andalusite hornfelses are present in the contact aureole of the Mansehra Granite in the Khaki and Darband area (Fig. 2f).

Petrography

The MGC magmatic rocks are mainly composed of microcline, plagioclase, quartz, biotite, and muscovite, whereas, zircon, apatite, tourmaline, chlorite, rutile, garnet, and ilmenite are accessories.

Microcline forms 20–50 vol.% of the Mansehra Granite (MG) and Hakale Granite (HG). Whereas the Leucogranite (LG) contains 3–20 vol.% microcline content. It is microperthitic, subhedral to anhedral, medium to coarse-grained, and shows cross-hatch twining (Fig. 3a). Myrmekites developed at the contact of plagioclase and microcline (Fig. 3g).

The quartz content of the MG, HG, and LG ranges between 30 and 43 vol.%. Fine to medium-grained, subhedral to anhedral grains are variably strained and show undulose extinction (Fig. 3d). Undulatory extinction of quartz and deformed micaceous folia suggest subsolidus deformation. Generally, these quartz grains are interlocked and exhibit mosaic texture. At places strained and microfractured quartz grains have sutured margins. Albite constitutes 15–35 vol.% of the MG and HG. However, the LG contains relatively higher (43–60 vol.%) albite content. It is subhedral to anhedral, fine to medium-grained, and shows polysynthetic twinning.

MG contains relatively higher biotite content which varies from 2 to 12 vol.% as compared with HG (2–6 vol.%) and LG (1–5 vol.%). It is pleochroic having straw-yellow to reddish-brown colour, occurs as randomly oriented subhedral flakes and encloses subhedral to euhedral zircon of size range from 100 to 150 μm and surrounded by dark haloes (Fig. 3b). Muscovite is found as 1–2 mm flakes in conjunction with biotite which shows bending and stretching due to stress

Fig. 2 Represents field features and contact relationships of various rocks from the Mansehra area exposed in the NW Himalaya. **a** Deformed K-feldspar phenocrysts and quartz swirled by mica **b** Psammitic xenoliths in Mansehra Granite, Mansehra area **c** Intrusion of Mansehra Granite (MG) into the metasediments of Tanawal Formation (TF) in Khaki **d** Contact of Mansehra Granite with the Tanawal Formation in Khaki **e** Migmatites near the contact of Mansehra Granite and Tanawal Formation in Khaki **f** Banded andalusite hornfelses developed near the contact of Mansehra Granite and Tanawal Formation in Darband

(Fig. 3c). Sericitization is commonly in albite and microcline (Fig. 3c).

Tourmaline (1–2 vol.%) occurs as subhedral to anhedral crystals of size range between 0.5 and 2.0 mm in MG, while LG contains 2–3 vol.% tourmaline (Fig. 3d). However, HG contains relatively higher tourmaline content (~5 vol.%). It replaces biotite, muscovite, and feldspar. Euhedral to subhedral apatite (0.5 vol.%) found enclosed in biotite (Fig. 3e–f). Anhedral Ilmenite (0.5 vol.%) and garnet are very occasionally observed in these granitic rocks (Naeem 2013).

The Tanawal Formation is principally composed of quartz, muscovite, biotite, whereas zircon and tourmaline occur as accessory minerals. Quartz ranges between 28.0 and 64.0 vol.% and its grain size varies from 0.05 to 1.00 mm. Strained and microfractured quartz indicates marginal

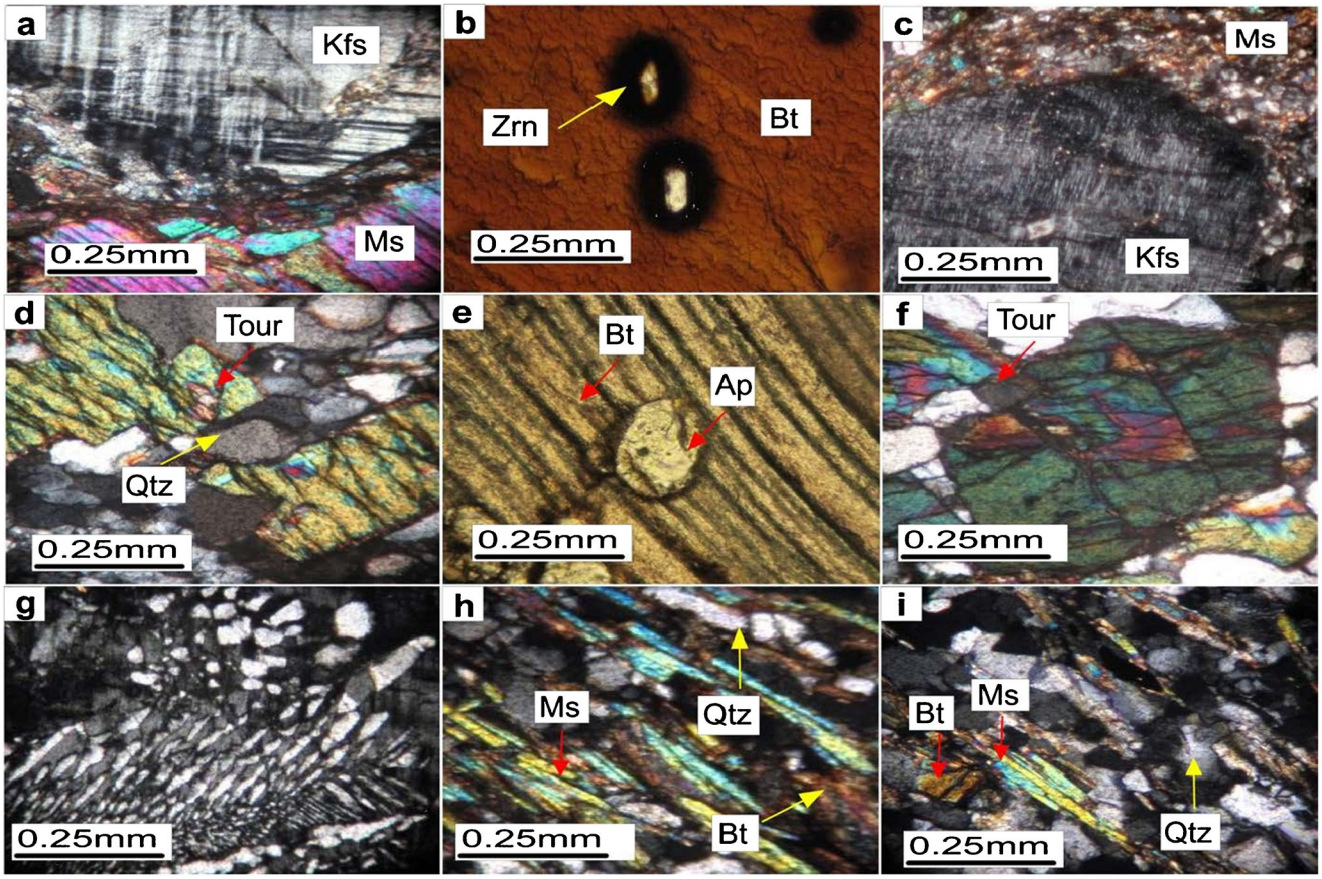

Fig. 3 Photomicrographs showing mineralogical and textural features in Mansehra Complex. **a** Cross-hatched microcline (Kfs) replaced by fine-grained muscovite (Ms) at the margin, associated with biotite (Bt) flakes **b** biotite flake encloses zircon (Zrn) crystals bounded by dark haloes **c** Microcline crystal invaded by fine muscovite in contact sample between Mansehra Granite and Hakale Granite **d** Tourmaline (Tour) crystals with strained quartz (Qtz) grains in Leucogranites **e-g** Presence of apatite (Ap), tourmaline and development of myrmekites in Hakale Granite **h** Alternate bands of biotite flakes and quartz grains in pelites of Tanawal Formation **i** Biotite flakes and quartz grains in psammites of Tanawal Formation

mylonization. Muscovite and biotite are in the range of 15–62 vol.% and 3–12 vol.%, respectively. Parallel to the subparallel alignment of deformed light-brown biotite flakes manifests tectonic foliation. Mica-rich and quartz-rich bands characterize pelites and psammites (Fig. 3h–i).

Fine-grained quartz is the principal constituent of psammites, whereas muscovite and biotite are subordinate components of the rock. In addition, 0.2 to 0.5 vol.% subhedral to euhedral zircon crystals (100–120 μm) are enclosed in dark brown biotite. The pelites of the Tanawal Formation are fine to medium-grained and comprised mainly of muscovite, biotite, chlorite, and quartz. K-feldspar and albite/oligoclase are ubiquitous accessory minerals. Tourmaline occurs as a randomly distributed accessory mineral, while apatite, ilmenite, and monazite are found in traces. The psammites range from almost pure quartz to micaceous quartzites with subordinate mica, K-feldspar, and albite.

Analytical techniques

Representative 40 samples of Mansehra Granite, Hakale Granite, and Leucogranites, each weighing about 5 kg were collected in Jhargali, Susalgali-Khaki, Oghi-Darband, Karkale, and Mansehra areas (Fig. 4). About 200 g of each sample was powdered in TEMA tungsten carbide grinding mill for chemical analysis. For major elements, fused lithium tetraborate discs were prepared following the method of Norrish and Hutton (1969). For the determination of trace elements, moisture-free pulverized rock sample was mixed with lithium tetraborate and pressed pellets were prepared by using a fusion machine (Phoenix 4000 VFD, Australia). Major and trace elements contents were determined by using wavelength-dispersive XRF spectrometer Pw 4400/24 Axios, PANalytical, Netherlands. Necessary corrections for matrix effect and the spectral overlapping were

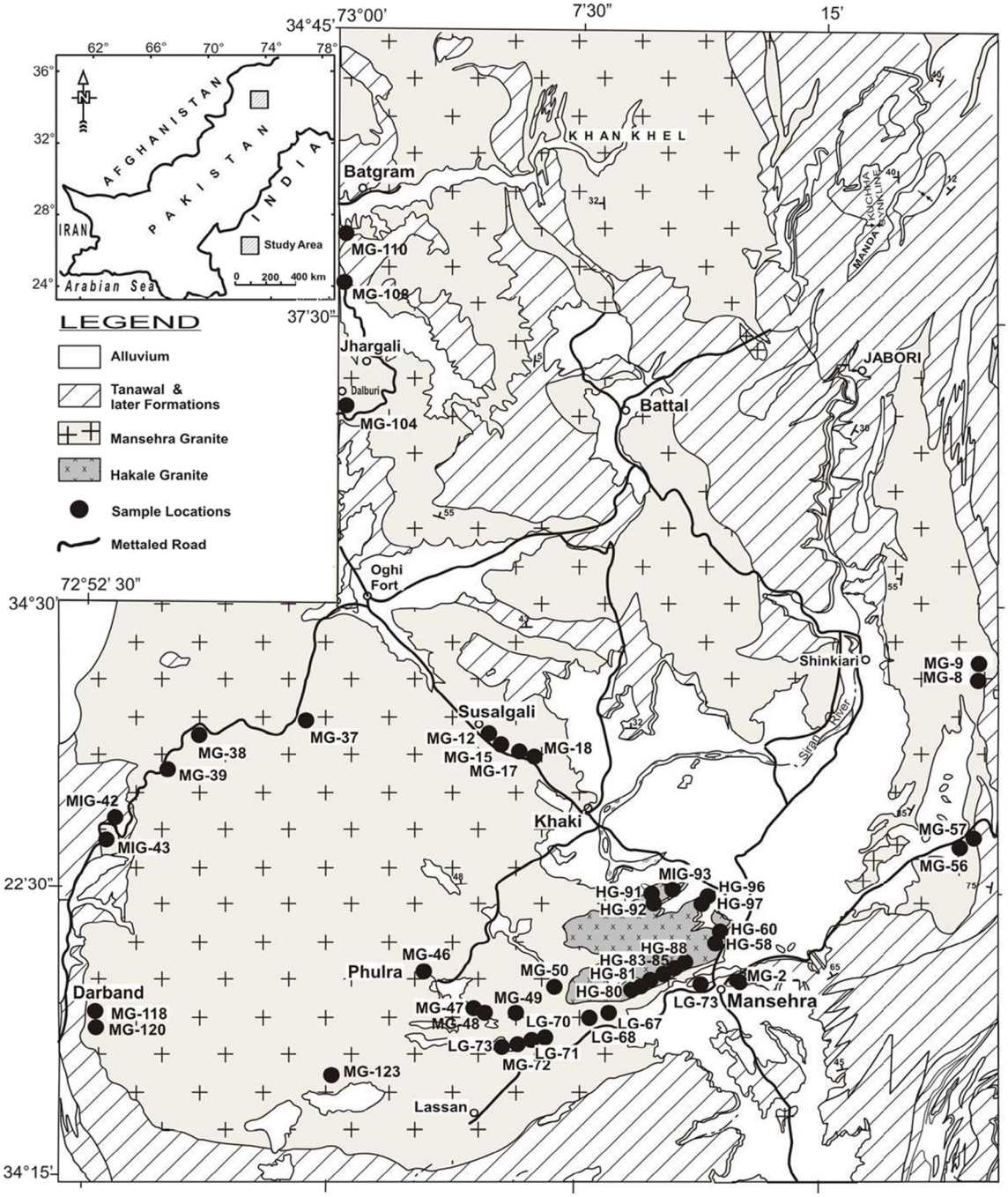

Fig. 4 Geological map of Mansehra area (from Zafar et al. 2019)

employed. Loss on Ignition (LOI) was determined by taking 5.0 g of each sample in a platinum crucible and heating at 1050 °C for 6–8 h in a muffle furnace. FeO was determined by the standard titration method following Furman (1962). Some of the major elements (Na, K) were evaluated by using a duly standardized Atomic Absorption Spectrometer (Thermo Scientific iCE 3000 Series, UK).

Analytical results and geochemistry

Major oxides and trace elements contents of 40 samples were determined and results are presented in Tables 1–2. The significantly higher value of Na_2O (mean 5.82%) in LG may correspond to its greater modal albite contents (Zafar et al. 2019). Average K_2O contents in MG and HG are around 5% however, lower K_2O value in LG is related to lesser modal

Table 1 Major oxides (%) and their ratios in Mansehra Granite (MG), Hakale Granite (HG), and Leucogranites (LG)

Samples	SiO_2	TiO_2	Al_2O_3	Fe_2O_3	FeO	MgO	CaO	K_2O	Na_2O	MnO	P_2O_5	LOI	Sum	A/CNK	A/NK	Na_2O/K_2O	K_2O/Na_2O	CaO/Na_2O	SiO_2/Al_2O_3
MG-2	70.50	0.63	15.07	2.00	1.11	1.23	1.55	4.17	2.69	0.08	0.20	0.75	99.98	1.791914	2.196793	0.65	1.55	0.58	4.68
MG-8	71.36	0.68	14.77	2.01	0.89	1.30	1.64	3.39	2.84	0.05	0.22	0.81	99.96	1.876747	2.370787	0.84	1.19	0.58	4.83
MG-9	70.05	0.64	15.05	2.04	1.25	1.26	1.59	4.25	2.75	0.13	0.21	0.70	99.92	1.752037	2.15	0.65	1.55	0.58	4.65
MG-12	72.09	0.37	14.49	1.28	1.65	0.61	1.08	4.51	2.92	0.07	0.19	0.67	99.93	1.702703	1.950202	0.65	1.54	0.37	4.98
MG-15	69.38	0.70	14.81	2.60	1.80	1.25	1.68	4.40	2.51	0.05	0.18	0.61	99.97	1.724098	2.143271	0.57	1.75	0.67	4.68
MG-17	70.20	0.36	16.54	0.36	1.25	0.70	0.99	5.41	3.28	0.09	0.19	0.57	99.94	1.708678	1.903337	0.61	1.65	0.30	4.24
MG-18	69.73	0.61	15.05	1.90	2.01	1.10	1.53	4.63	2.75	0.08	0.24	0.34	99.97	1.689113	2.039295	0.59	1.68	0.56	4.63
MG-37	72.08	0.63	15.22	0.10	1.61	0.22	0.48	4.82	3.77	0.08	0.27	0.70	99.98	1.67806	1.771828	0.78	1.28	0.13	4.74
MG-38	70.12	0.32	16.21	1.10	1.49	0.59	1.35	4.81	3.20	0.09	0.10	0.58	99.96	1.731838	2.02372	0.67	1.50	0.42	4.33
MG-39	70.04	0.70	14.22	2.13	2.05	1.26	1.69	4.34	2.53	0.08	0.18	0.73	99.95	1.661215	2.069869	0.58	1.72	0.67	4.93
MG-46	71.22	0.67	14.31	1.25	1.01	2.01	1.54	4.10	3.07	0.11	0.37	0.31	99.97	1.642939	1.995816	0.75	1.34	0.50	4.98
MG-47	71.52	0.45	15.32	0.64	2.03	0.77	1.23	4.55	2.70	0.10	0.18	0.49	99.98	1.806604	2.113103	0.59	1.69	0.46	4.67
MG-48	70.16	0.58	15.04	0.89	1.72	1.17	1.47	4.71	3.48	0.05	0.24	0.43	99.94	1.556936	1.836386	0.74	1.35	0.42	4.66
MG-49	72.13	0.44	15.12	0.42	1.43	0.77	1.10	4.71	2.86	0.10	0.19	0.58	99.85	1.743945	1.997358	0.61	1.65	0.38	4.77
MG-50	72.01	0.44	14.13	0.61	2.86	0.82	1.27	4.15	2.63	0.09	0.17	0.76	99.94	1.75528	2.084071	0.63	1.58	0.48	5.10
MG-56	70.56	0.44	15.16	0.72	1.80	0.88	1.07	4.63	3.53	0.07	0.24	0.87	99.97	1.64247	1.857843	0.76	1.31	0.30	4.65
MG-57	69.6	0.54	15.18	0.72	1.95	1.13	1.68	4.68	3.40	0.04	0.22	0.80	99.94	1.555328	1.878713	0.73	1.38	0.49	4.58
MG-72	69.78	0.80	14.02	1.38	1.91	1.83	1.19	2.01	3.02	0.08	0.33	0.61	96.96	2.254019	2.787276	1.50	0.67	0.39	4.98
MG-104	72.11	0.79	15.00	0.56	0.98	1.20	1.83	4.09	2.81	0.07	0.17	0.36	99.97	1.718213	2.173913	0.69	1.46	0.65	4.81
MG-108	70.06	0.78	16.45	0.61	1.22	1.37	1.81	4.11	2.94	0.06	0.21	0.33	99.95	1.856659	2.333333	0.72	1.40	0.62	4.26
MG-110	74.12	0.53	14.32	0.45	0.96	1.06	1.41	4.02	2.59	0.07	0.08	0.28	99.89	1.785536	2.166415	0.64	1.55	0.54	5.18
MG-118	72.75	0.26	15.39	0.31	0.92	0.63	0.99	4.28	3.25	0.05	0.22	0.89	99.94	1.806338	2.043825	0.76	1.32	0.30	4.73
MG-120	72.01	0.57	15.02	0.49	0.89	1.01	1.50	4.99	2.52	0.08	0.19	0.68	99.95	1.667037	2	0.51	1.98	0.60	4.79
MG-123	70.11	0.53	16.3	0.45	1.12	0.78	1.14	6.36	2.18	0.06	0.16	0.77	99.96	1.683884	1.908665	0.34	2.92	0.52	4.30
HG-58	70.48	0.29	16.4	0.54	1.02	0.92	1.16	4.45	3.72	0.09	0.23	0.67	99.97	1.757771	2.007344	0.84	1.20	0.31	4.30
HG-60	72.25	0.53	14.94	0.46	0.92	0.94	1.19	4.86	2.80	0.05	0.19	0.82	99.95	1.688136	1.950392	0.58	1.74	0.43	4.84
HG-80	72.33	0.43	15.13	0.68	0.92	0.78	1.18	4.85	2.89	0.03	0.17	0.53	99.92	1.696188	1.95478	0.60	1.68	0.41	4.78
HG-81	73.26	0.43	14.86	0.65	0.91	0.75	1.10	4.36	2.72	0.09	0.17	0.67	99.97	1.816626	2.09887	0.62	1.60	0.40	4.93
HG-83	71.55	0.45	15.56	0.56	1.06	0.74	1.33	5.29	2.66	0.06	0.19	0.49	99.94	1.676724	1.957233	0.50	1.99	0.50	4.60
HG-84	69.62	0.51	14.43	0.83	2.76	1.14	1.48	5.41	2.63	0.07	0.28	0.76	99.92	1.515756	1.794776	0.49	2.06	0.56	4.82
HG-85	70.01	0.53	15.32	0.50	1.14	0.96	1.45	5.30	3.51	0.09	0.23	0.90	99.94	1.493177	1.738933	0.66	1.51	0.41	4.57
HG-88	73.3	0.47	15.13	0.69	0.64	0.82	1.30	4.00	2.57	0.09	0.18	0.78	99.97	1.92249	2.302892	0.64	1.56	0.51	4.84
HG-91	74.57	0.19	14.81	0.40	0.24	0.32	0.90	5.36	2.09	0.04	0.34	0.67	99.93	1.773653	1.987919	0.39	2.56	0.43	5.04
HG-92	72.12	0.33	15.95	0.74	0.69	0.52	1.05	4.49	3.15	0.04	0.26	0.62	99.96	1.835443	2.087696	0.70	1.43	0.33	4.52
HG-96	71.52	0.13	16.6	0.34	0.62	0.20	0.51	5.10	3.53	0.07	0.29	1.01	99.92	1.816193	1.923523	0.69	1.44	0.14	4.31
HG-97	71.22	0.18	17.02	0.87	0.67	0.38	0.80	3.18	4.20	0.09	0.31	1.02	99.94	2.080685	2.306233	1.32	0.76	0.19	4.18
LG-67	74.28	0.16	16.14	0.14	0.48	1.23	0.12	1.87	5.23	0.02	0.03	0.27	99.97	2.235457	2.273239	2.80	0.36	0.02	4.60
LG-70	70.32	0.11	17.18	0.11	0.54	0.63	0.92	2.26	6.19	0.01	0.58	1.11	99.96	1.833511	2.033136	2.74	0.37	0.15	4.09
LG-71	73.53	0.16	16.15	0.14	0.52	1.23	0.12	1.87	5.24	0.01	0.03	0.94	99.94	2.233748	2.271449	2.80	0.36	0.02	4.55
LG-73	72.50	0.63	16.53	0.08	0.38	0.42	0.54	1.77	6.52	0.01	0.28	0.29	99.95	1.872027	1.993969	3.68	0.27	0.08	4.39

Table 2 Trace elements (ppm) and their ratios in Mansehra Granite (MG), Hakale Granite (HG), and Leucogranites (LG)

Samples	Rb	Sr	Ba	Y	Zr	Nb	Sn	Cs	Pb	Th	U	Rb/Sr	Rb/Ba	Sr/Ba	Nb/Th
MG-2	233	81	272	33	184	16	32	8	25	55	11	2.88	0.86	0.30	0.29
MG-8	283	68	251	28	145	15	33	24	25	51	24	4.16	1.13	0.27	0.29
MG-9	248	60	354	25	134	14	38	16	29	49	12	4.13	0.70	0.17	0.29
MG-12	203	78	347	31	163	14	30	13	21	53	14	2.60	0.59	0.22	0.26
MG-15	144	168	216	18	125	13	32	9	11	46	12	0.86	0.67	0.78	0.28
MG-17	239	48	285	21	94	13	31	7	27	44	13	4.98	0.84	0.17	0.30
MG-18	233	79	377	28	163	16	27	2	25	54	12	2.95	0.62	0.21	0.30
MG-37	183	74	360	24	151	13	30	1	29	49	12	2.47	0.51	0.21	0.27
MG-38	179	53	237	21	85	9	28	n.d.	28	41	15	3.38	0.76	0.22	0.22
MG-39	208	89	320	30	201	16	30	3	27	57	13	2.34	0.65	0.28	0.28
MG-46	230	63	245	31	158	15	32	18	23	54	11	3.65	0.94	0.26	0.28
MG-47	259	56	282	28	122	13	35	12	25	49	13	4.63	0.92	0.20	0.27
MG-48	289	54	250	27	125	15	35	12	30	52	23	5.35	1.16	0.22	0.29
MG-49	260	50	264	28	120	14	37	12	26	49	12	5.20	0.98	0.19	0.29
MG-50	238	54	204	27	128	14	30	19	22	51	13	4.41	1.17	0.26	0.27
MG-56	278	53	356	22	110	14	36	32	31	49	13	5.25	0.78	0.15	0.29
MG-57	328	47	184	20	93	15	35	21	39	48	23	6.98	1.78	0.26	0.31
MG-72	235	58	240	26	131	14	35	5	24	49	14	4.05	0.98	0.24	0.29
MG-104	208	109	530	48	281	20	33	10	14	57	bdl	1.91	0.39	0.21	0.35
MG-108	194	72	417	35	188	16	33	7	16	50	20	2.69	0.47	0.17	0.32
MG-110	208	62	360	42	315	18	35	2	28	65	19	3.35	0.58	0.17	0.28
MG-118	240	53	267	25	107	13	37	1	19	45	24	4.53	0.90	0.20	0.29
MG-120	207	63	234	33	185	18	34	17	14	58		3.29	0.88	0.27	0.31
MG-123	218	60	327	30	164	16	33	13	18	53	23	3.63	0.67	0.18	0.30
HG-58	244	56	219	27	121	13	35	15	23	50	14	4.36	1.11	0.26	0.26
HG-60	194	49	286	24	100	12	35	16	18	47	10	3.96	0.68	0.17	0.26
HG-80	267	62	295	29	128	14	38	11	27	51	13	4.31	0.91	0.21	0.27
HG-81	246	72	268	30	138	14	34	3	24	52	13	3.42	0.92	0.27	0.27
HG-83	293	68	295	27	131	15	36	7	28	53	23	4.31	0.99	0.23	0.28
HG-84	282	72	422	26	111	12	38	23	29	48	14	3.92	0.67	0.17	0.25
HG-85	237	61	303	26	115	13	38	15	25	50	13	3.89	0.78	0.20	0.26
HG-88	256	55	293	27	126	14	36	5	24	51	12	4.65	0.87	0.19	0.27
HG-91	374	20	113	21	38	16	53	45	22	38	13	18.70	3.31	0.18	0.42
HG-92	394	23	139	20	40	16	53	36	27	38	14	17.13	2.83	0.17	0.42
HG-96	407	22	145	21	47	16	58	76	28	37	13	18.50	2.81	0.15	0.43
HG-97	263	90	168	17	51	17	58	28	8	39	14	2.92	1.57	0.54	0.44
LG-67	21	16	28	52	125	17	31	-	-	53	-	1.31	0.75	0.57	0.32
LG-70	163	20	65	12	31	14	56	9	-	35	23	8.15	2.51	0.31	0.40
LG-71	116	11	42	4	50	13	51	-	-	38	23	10.55	2.76	0.26	0.34
LG-73	163	20	65	12	31	14	56	9	-	35	23	8.15	2.51	0.31	0.40

microcline contents. Lower CaO and Na_2O contents relative to K_2O are due to lesser modal plagioclase and higher microcline contents of the MGC (Zafar et al. 2019). FeO contents vary widely reflecting the relative abundance of biotite in the respective rocks. The LG has the lowest FeO content because of its lesser biotite component. Variations in TiO_2 and MnO contents may correspond to accessory mineral levels in the MGC (Zafar et al. 2019). K_2O/Na_2O and CaO/Na_2O ranged from 0.27–2.92 to 0.02–0.67.

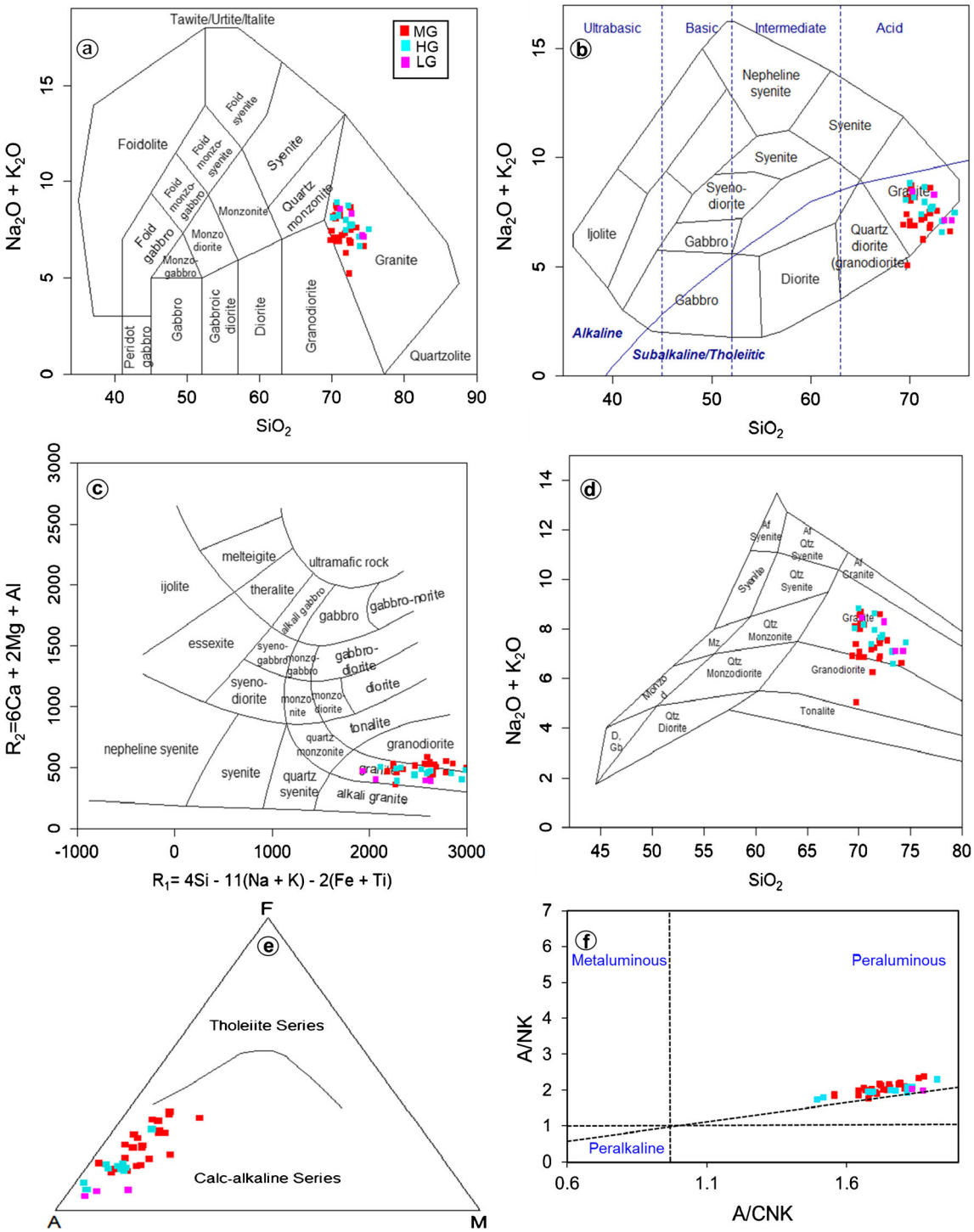

Fig. 5 Geochemical classification diagrams. **a** SiO_2-Na_2O+K_2O plot (Middlemost 1985) **b** total alkalis versus SiO_2 diagram (Cox et al. 1979) **c** R1-R2 plot (De La Roche et al. 1980) **d** TAS diagram (Middlemost 1994) **e** AFM diagram (Irvin and Baragar 1971) **f** A/CNK-ANK plot (Shand 1943) of Mansehra Granite, Hakale Granite and Leucogranites

Granitic rocks of the MGC are enriched in Rb and Ba relative to Sr. Average Ba, Rb, and Sr contents in MG, HG, and LG are in the range of 28–530, 21–407 ppm, and 11–168 ppm, respectively. Rb/Sr, Sr/Ba, Rb/Ba, and Nb/Th ratios, varied 0.86–18.70, 0.15–0.78, 0.39–3.31, and 0.22–0.44, respectively (Table 2). A/CNK values of MG and HG varied 1.49–2.25 (Table 1), which suggest peraluminous to the highly peraluminous felsic character of the MGC magmatic rocks.

Chemical data of the MG, HG, and LG was plotted in total alkali versus silica which placed these rocks in the granite field

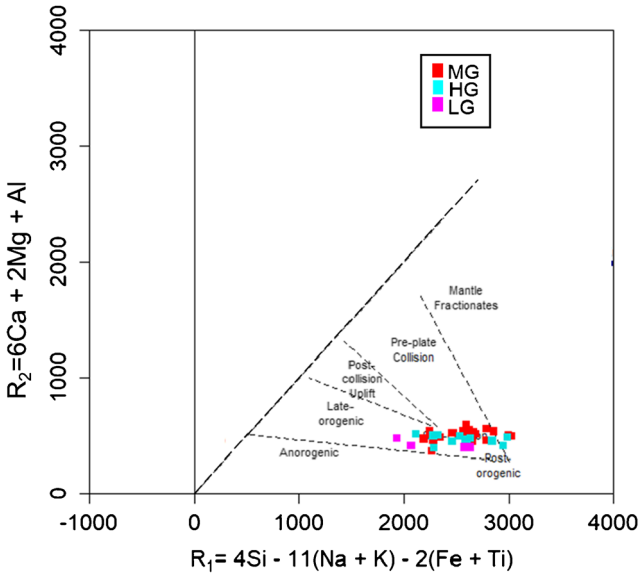

Fig. 6 R1-R2 (Batchelor and Bowden 1985) plot of chemical data of the MG, HG, and LG in geotectonic discrimination diagram indicating syn-orogenic setting

(Fig. 5a–d). However, a few samples lie in the granodiorite region due to minor local compositional variations. Using the AFM diagram, all the samples are of calc-alkaline compositions (Fig. 5e). Based on A/CNK versus the A/NK plot, these granites are peraluminous (Fig. 5f). The plot of chemical data of the MG, HG, and LG in geotectonic discrimination diagrams placed these granitoids in syn-orogenic, continental-continental collisional fields (Figs. 6–7).

Harker's variation plots and spider diagrams

Major oxides and trace elements data of the MG, HG, and LG were plotted in Harker's variation diagrams. Some of the variation diagrams of major oxides reveal scattering. Major oxide (FeO) show a negative correlation with SiO_2 in MG, HG, and LG (Fig. 8a). However, a weak negative trend is indicated by Sr with SiO_2 (Fig. 8b). In addition, Zr exhibits a positive correlation with MgO (Fig. 8c). The trace elements Th and Y demonstrate a significant positive correlation with Zr (Fig. 8d–e). Likewise, the Ba–Sr plot displays a significant positive trend as presented in Fig. 8f.

Primitive mantle normalized Spider diagrams show that the MG is enriched in Rb, K, Pb, U, and Nd, and depleted in Ba, Sr, Ti, Nb, Ce, and La (Fig. 9). The HG has strong positive anomalies of Rb, K, Pb, and weak positive variation of Nd and P. Sr, Ba, Ti, and Nb show strong negative trends and relatively poor inverse variation of La. While, the LG displayed a positive trend for Rb, Pb, Th, Nd, Zr and negative variation of Ba, Sr, Ti, and Nb.

Zircon saturation thermometry

Accessory minerals furnish useful information regarding geochemical variation during partial melting of rocks (e.g., Hoskin et al. 2000). During crystallization of granitic melt, abundances of incompatible elements are gradually increased and ultimately accumulated in accessory minerals like zircon and monazite. Concentrations of these minerals are controlled by their solubility in the felsic melt which is a function of magma temperature (Mills et al. 2008). The saturation behaviour of these minerals can be used to determine the temperature of magma (Miller et al. 2003; Janousek et al. 2006). Zircon commonly occurs as an accessory mineral in magmatic rocks (Hoskin and Schaltegger 2003).

Petrographic study of the MGC magmatic rocks indicates the presence of euhedral zircon crystals in these rocks. Euhedral zircon crystals found in granites are magmatic and can be used to estimates the crystallization temperature of granitic melt (Watson and Harrison 1983). Compositional data of the MGC magmatic bodies was used to estimate the crystallization temperatures of these rocks by using software GCDKIT (Janousek et al. 2006) employing the technique reviewed by Hancher and Watson (2003). The method was applied with the assumption that zircon has no extraneous source, homogeneously distributed and zircon crystallized close to the liquidus (Janousek et al. 2006). Mean zircon temperatures of the MGC rocks are presented in Table 3.

Discussion

Field features and petrological characteristics of granitic rocks

The Mansehra Granite is generally massive but occasionally gneissic due to local shearing manifested by superimposed tectonic foliation. Mica flakes swirled around augen-shaped K-feldspar phenocrysts and deformed quartz suggests signatures of tectonic deformation (Fig. 2a). Similar deformational characteristics are also exhibited by granites found in the Himalayas of Nepal, Sikkim, Bhutan, and India (e.g., Singh 2010). Due to higher silica contents (Table 1), the MG and HG are enriched in quartz which is more susceptible to deformation than K-feldspar. Therefore, deformation, foliation, and gneissic character are common features of these granites. MG and HG contain K-feldspar phenocrysts that are microcline, which is not stable at magmatic temperatures and crystallized from the granitic melt as a primary mineral phase at relatively lower temperatures (Kerrick 1969). Hence, initial cooling of the MGC magma most likely had initiated the

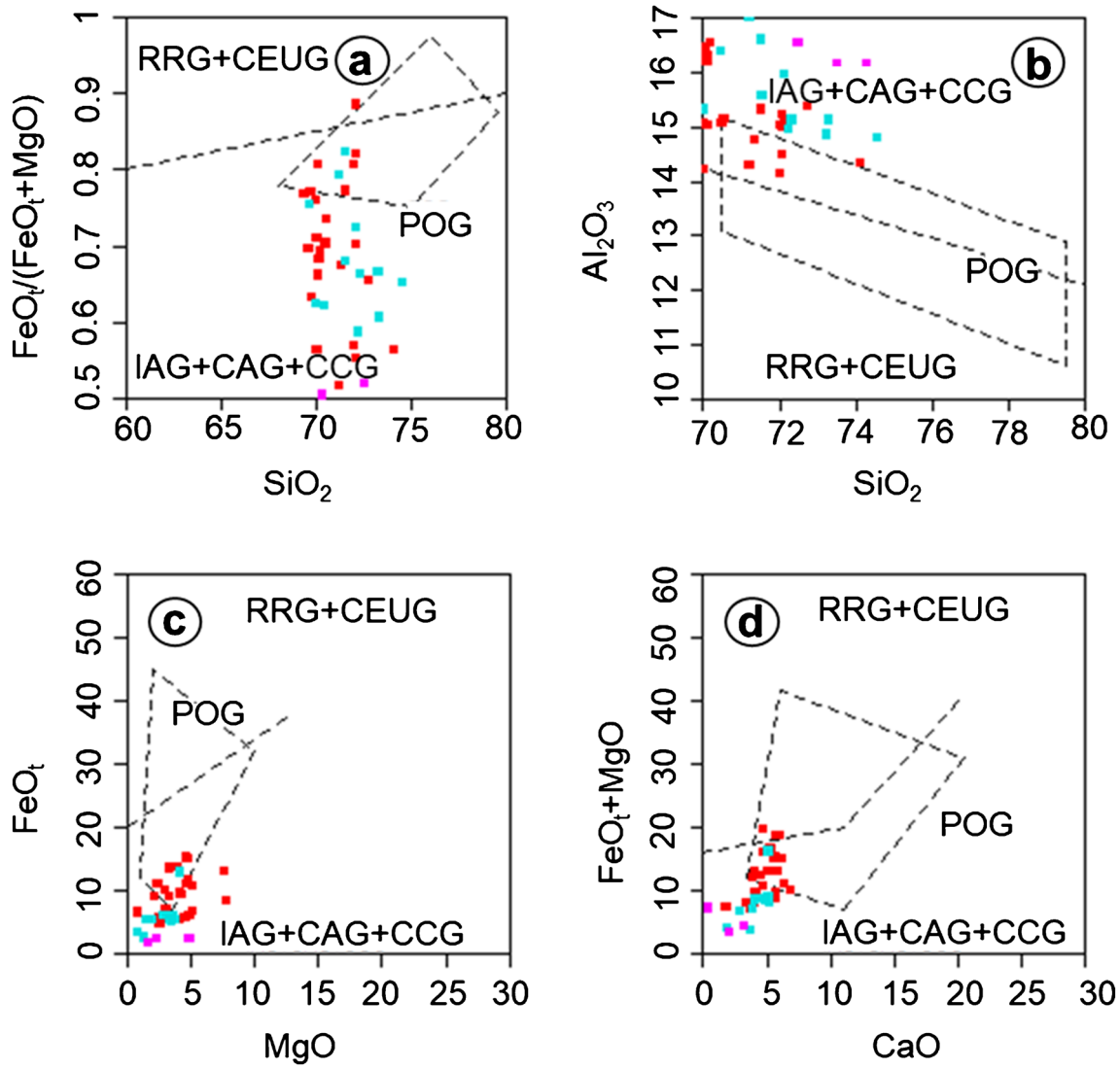

Fig. 7 Plot of the chemical composition of Mansehra Granite, Hakale Granite, and Leucogranites in tectonic discrimination diagrams (Maniar and Piccoli 1989). Abbreviations: IAG (Island Arc Granitoids), CAG (Continental Arc Granitoids), CCG (Continental Collision Granitoids), POG (Post-orogenic Granitoids), RRG (Rift-related Granitoids), CEUG (Continental Epeirogenic Uplift Granitoids), OP (Oceanic Plagiogranites)

growth of large K-feldspar phenocrysts. Subsequently, due to shallower emplacement, the granitic melt crystallized at a faster rate and constituted medium-grained groundmass which imparted the porphyritic/sub-porphyritic texture to the MG and HG.

In addition to K-feldspar phenocrysts, the Mansehra Granite also contains restites of variable size and composition which indicate limited assimilation of the source rock "Tanawal Formation" in the granitic melt (Fig. 2b; Zafar et al. 2019). The presence of restites and migmatites suggests the anatectic nature and S-type character of the MGC magmatic rocks (Fig. 2b, e). The occurrence of migmatites, metapelites, and gneissic rocks along with the presence of Al-rich minerals especially muscovite and garnet, apatite, ilmenite as well as monazite, and absence of accessory minerals magnetite, allanite, and titanite also reveal S-type features of the MGC (Fig. 2e, Fig. 3a–f; Khan et al. 2019). Moreover, the presence of brown to reddish-brown pleochroic biotite along with ilmenite and discrete crystals of apatite further validate the S-type trait of the MGC (Fig. 3b, e).

During the cooling of magma, biotite crystallizes at an earlier stage, whereas muscovite formed at a shallower depth and relatively lower temperature (Best 2003). The MG contains biotite>muscovite as compared with HG having muscovite>biotite due to crystallization of the latter at the upper crustal level and relatively lower temperature. Comparatively higher tourmaline contents of HG (~5%) suggest higher boron concentration that might have lowered the solidus temperature of the melt resulting in the crystallization of muscovite. After shallow emplacement and predominant

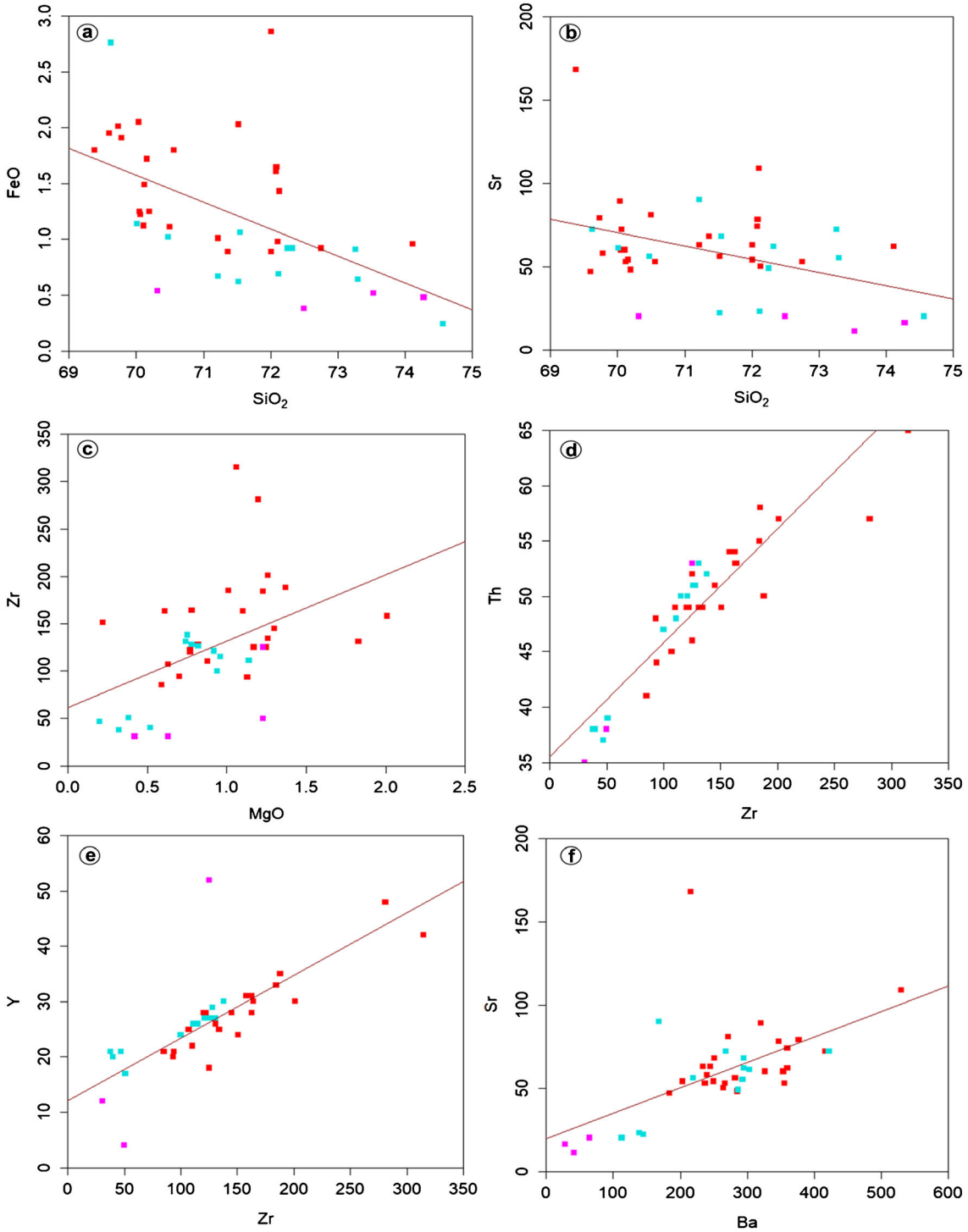

Fig. 8 Harker's Variation diagrams of major oxides and trace elements in Mansehra Granite, Hakale Granite, and Leucogranites

crystallization of the HG, the fluid-rich melt most likely moved to a relatively higher crustal level with a consequent increase in vapour pressure and insurgent boiling. This phenomenon most probably had induced fracturing and subsequent quenching of this fluid-rich residual melt which rendered the fine-grained nature of the microgranitic bodies. These microgranites are devoid of K-feldspar phenocrysts.

In the course of crystallization of MGC magma, the residual melt most likely got progressively enriched in water and generated Na_2O-rich granitic melt. Ultimately this phase got

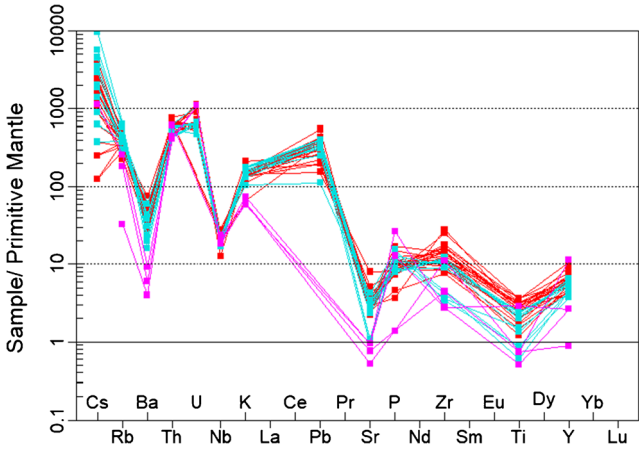

Fig. 9 Spider diagram of Mansehra Granite, Hakale Granite, and Leucogranite

separated and crystallized sodic leucogranitic bodies in the Mansehra area. These bodies contain higher mean Na_2O contents (5.82%) as compared with MG (2.92%) and HG (3.03%), and correspondingly higher modal albite (up to 60%) relative to MG (15–20%) and HG (15–35%). Relatively gradual cooling of the low-temperature residual melt may have enough time to exsolve most of the Na as albite in leucogranites which is consistent with the observations of Nagudi et al. (2003).

Zircon saturation temperatures

Zircon saturation temperatures of the MG range between 749 and 852 °C (average 790 °C). Whereas, the estimated temperature of the migmatites in Susalgali-Khaki is 803 °C which is comparable with the average temperature of 813 °C at the contact between Mansehra Granite and metasediments of the Tanawal Formation. Crystallization temperature at the contact of HG with MG is 726 °C. While zircon saturation temperatures of HG varied from 709 to 779 °C (mean 744 °C). Crystallization temperatures of the leucogranites are in the range of 749–754 °C (mean 751 °C) in the Mansehra-Phulra area (Table 3). The HG contains tourmaline-bearing microgranitic bodies in Maswal and Oghi-Darband areas having crystallization temperatures of 691 °C and 692 °C that is comparable with the estimated temperatures of the HG (Naeem 2013). The occurrence of tourmaline in microgranites most likely has lowered the crystallization of these bodies.

The fluid-absent melting of pelite-psammite bearing metasediments begins at temperatures below 800 °C, usually around 750 °C (e.g., Vielzeuf and Schmidt 2001). However,

Table 3 Zircon saturation temperatures of Mansehra Granite, Hakale Granite, Leucogranites, Migmatites, and Mansehra Granite-Tanawal Formation, Mansehra Granite-Hakale Granite contacts (Naeem 2013)

Rock type	Area	Average Zircon Sat. Temp °C
Mansehra Granite	Attar-Batrasi	749
	Oghi-Darband	774
	Susalgali-Khaki	779
	Mansehra-Phulra	785
	Mansehra-Balakot	786
	KKH	786
	Darband-Lassan	794
	Mansehra	801
	Oghi-Jhargali	852
Mean value		790
Hakale Granite	Mansehra-Maswal	709
	Mansehra	779
Mean value		744
Leucogranites	Mansehra-Karkale	749
	Mansehra	754
Mean value		751
Migmatites	Susalgali-Khaki	803
	Susalgali-Khaki	863
Mean value		833
Mansehra Granite-Tanawal Formation contact	Mansehra-Balakot	794
	Susalgali-Khaki	832
Mean value		813
Mansehra Granite-Hakale Granite contact	Mansehra	726

experimental work of various researchers suggests that fluid-absent partial melting of metasediments occurs at 800 °C or even higher temperatures (850 °C) (Clemens and Watkins 2001; Johnson et al. 2001). Melting of biotite commenced around 780–820 °C at 5 kbr whereas, 700–800 °C temperature range has been proposed for dehydration-melting of muscovite (Janasi and Martins 2003; Garcia-Casco et al. 2003). Mean temperature (813 °C) of MG at the contact with metasediments of Tanawal Formation and migmatites (803 °C) in the Susalgali-Khaki area are consistent with biotite dehydration-melting temperatures. However, a relatively lower mean temperature of 744 °C of HG suggests the genesis of this granitic body due to muscovite dehydration-melting (Table 3). Based on two-feldspar geothermometry crystallization temperature range of 600–700 °C was suggested for the MG (Shams and Rehman 1967), which is lower than the dehydration-melting temperature of pelite-psammite bearing metasediments.

The current study reflects that MG magma most probably has been generated by biotite dehydration-melting at > 5 kbr pressure and > 700 °C temperature, while the ascent of magma at shallow levels most likely has initiated localized muscovite fluid-absent melting and generated HG magma. Tourmaline formed at 725 °C and 6 kbr in subsolidus to near-solidus conditions which is consistent with the mean temperature of 744 °C for HG.

Mean estimated temperatures of the MGC magmatic rocks are comparable with the temperature range of 800–850 °C obtained from S-type granites of the eastern Lachlan Fold Belt (Mass et al. 1997). Zircon saturation temperatures of Lesser Himalayan granites of India varied in the range of 690–817 °C for Mandi granites, 680–750 °C for Kaplas, 670–780 °C for Chamba-Kullu, 743–815 °C for Chandra, 705–802 °C for Nyimaling, and 700–815 °C for Kinnaur Kaila (Miller et al. 2001). These temperatures are closer to the dehydration-melting of biotite Patino-Douce and Johnston (1991). Mean zircon temperatures of HG (744 °C) and MG (790 °C) are comparable with the temperature range of S-type granites found in the Lesser Himalayan Granite Belt of India (Table 3).

Petrogenesis

Geochemical classification diagrams placed MG, HG, and LG in calc-alkaline, peraluminous granitoid field (Fig. 5). More than 1.1 A/CNK values and corundum normative character indicate the peraluminous nature of magmatic bodies of the MGC. Peraluminous granitic melts have low Ti solubility and their higher concentrations lead to the stability of biotite (Pickering and Johnston 1998). Owing to relatively higher Ti concentration the MG contains more biotite as compared with HG due to lower Ti contents.

Negative trends of major oxide (FeO) and trace element (Sr) with SiO_2 in MG, HG, and LG suggest crystallization of plagioclase and biotite from the granitic melt of the MGC (Fig. 8a–b). Positive variations in Ba–Sr plot (Fig. 8f) indicate fractionation of feldspar. The direct relationship between MgO and Zr (Fig. 8c) revealed that the melt was saturated with trace element Zr, which had crystallized accessory mineral zircon. Crystallization of zircon is geochemically favoured in peraluminous granitic melt containing lower CaO contents (Yurimoto et al. 1990) as in the case of MG (1.36%). Trace elements Zr, Hf, and Yb are concentrated in accessory mineral zircon which strongly influences the behaviour of rare earth elements (U, Th, Y, Nb) during the evolution of granitic magma (Belousova et al. 2006; Villaros et al. 2009). Due to large ions and high charges, these rare earth elements are not accommodated by major rock forming minerals and concentrate in the residue of the granitic magma where these are taken up by zircon. The direct relationship of Zr with Y and Th (Fig. 8d–e) reflects the accumulation of Y and Th in accessory mineral zircon. The decrease of TiO_2 and Zr with differentiation in MG and HG most likely indicates crystallization of rutile, ilmenite, and zircon from the melt.

Variation diagrams of the MG, HG, and LG display significant relationships which reveal imperfect mixing of the nonhomogenous protolith during partial crustal melting (Fig. 8). However, scattering in some of the plots reflects the heterogeneity of the protolith and irregular distribution of minerals in the granitic melt of the MGC, as argued by Singh and Kumar (2005). Strong negative Ba, Sr, and Ti anomalies in spidergrams of MG, HG, and LG most likely indicate crystallization of K-feldspar, plagioclase, biotite, and Fe-Ti oxides in these plutonic rocks (Fig. 9). Negative Sr and Ba anomalies suggest strong partitioning of Sr into K-feldspar and albite-rich plagioclase and Ba into micas and K-feldspar.

Mean Ba contents in MG (299 ppm), HG (245 ppm), and LG (57 ppm) correspond with average modal microcline contents (43, 30, and 12%) of these rocks. The wider variations in mean contents of Rb (21–407 ppm) and Sr (11–168 ppm) in plutonic rocks of the MGC reflect the non-homogenous distribution of modal K-feldspar and plagioclase in the granite protolith. Relatively higher contents of incompetent elements, Sn (27–58), Th (35–65), U (10–24), Pb (8–39), and Cs (1–76) ppm suggest that the magmatic bodies are derived by crystal fractionation of the granitic melt through partial crustal melting of metasediments (of the Tanawal Formation). However, lower Na, Ca, and Sr contents in MG and HG are due to the removal of these elements from the solutions during weathering of the protolith feldspar into clays and consequent enrichment of Rb, K, and Pb due to their incorporation in argillaceous component of the source (Tanawal Formation), as observed by Chappell and White (2001). Lower Na, Ca, and higher K, Rb contents in MG and HG correspond to their

lesser modal concentration of plagioclase (15–20%) as compared with K-feldspar (35–51%). However, owing to higher Na_2O values (up to 6.52%) the LG contains higher modal plagioclase contents (43–60%) relative to MG (15–20%) and HG (15–35%). The variation of plagioclase in MG and HG and mean Rb/Sr ratio (0.86 and 18.70) correspond to the erratic distribution of plagioclase retained in the residue during partial melting of the granite protolith.

Higher SiO_2 contents (69.38–74.57%), K_2O/Na_2O ratio (0.27–2.92), higher Rb concentration relative to Sr, Rb/Ba ratio > 0.25 and Nb/Th ratio (0.22–0.44) in addition to the presence of muscovite and biotite suggest that granitic melt of the MGC was likely derived from the crustal source (the Tanawal Formation) similar to the observation of Singh (2010). Low mean values of Na_2O and CaO, higher K_2O contents, enrichment of Ba and Rb relative to Sr, Rb/Ba ratio 0.39–3.31, Rb/Sr > 0.25 indicate pelitic source rock for the granitic melt of the MGC (Jung et al. 2000). CaO/Na_2O ratio in S-type granite is controlled by the plagioclase contents of the protolith. Peraluminous melt generated from clay-rich source rock (plagioclase poor) has lower CaO/Na_2O ratio (< 0.3) as compared with clay-poor (plagioclase-rich) source rock having CaO/Na_2O ratio > 0.3 (Sylvester 1998). Mean CaO/Na_2O ratio (0.02 and 0.67) in plutonic rocks of the MGC suggests mainly clay-rich heterogeneous source with subordinate plagioclase-rich component which may correspond to the predominant occurrence of pelite-psammite bands in metasediments of the host (the Tanawal Formation).

Comparable K_2O/Na_2O ratio in MG (1.54) and HG (1.63) together with $K_2O>Na_2O$ suggest derivation of the magmas of these plutonic bodies from a similar source rock of varied composition, as argued by Jung et al. (1999). The previously determined $^{87}Sr/^{86}Sr$ ratio of the MG (Le Fort et al. 1980) in the range of 0.727–0.847 (> 0.708 for S-type granites) is consistent with the heterogeneous source rock and S-type nature of the MGC. A fairly consistent mean SiO_2/Al_2O_3 ratio in MG (4.71), HG (4.64), and LG (4.34) also reveal the generation of granitic melt by partial crustal melting of the host rock, as shown by Regmi (2008). The Rb/Sr and Sr/Ba ratios indicate that granitic magma is derived by fluid-absent biotite melting (Harris and Inger 1992). The majority of Rb/Sr ratio in MGC is in close agreement with the Rb/Sr ratio (4–10) suggested by Harris et al. (1993) for the derivation of granitic magma by dehydration-melting of the protolith. Average Ba/Sr and Rb/Sr ratios (4.59 and 3.74), and Fe_2O_3 + MgO (2.08%) of MG also suggest that the granitic melt was derived most likely from the biotite dehydration-melting of source rock (the Tanawal Formation). However, the HG magma was probably generated at relatively higher crustal levels by muscovite fluid-absent melting, which is similar to the findings of Sharma and Rashid (2001). Lesser mean Fe_2O_3 (0.60%), MgO (0.70%), CaO (1.12%), Fe_2O_3 + MgO (1.31%) contents, Ba/Sr and higher Rb/Sr ratio (7.50) may indicate muscovite dehydration-melting of pelites-psammites (the Tanawal Formation in this case) which is consistent with the model proposed by Sharma and Rashid (2001) for similar rocks.

The presence of andalusite and perthitic microcline in granitic rocks indicates shallow depth of emplacement (Pant and Kundu 2008; Singh 2010). Likewise, the occurrence of andalusite in the contact aureole of the MG along with the presence of perthitic microcline suggests that the MGC magma was emplaced at shallow (less than 14 km) depth. Upper crustal (5–15 km) signatures of the MGC are also depicted by negative Nb, Sr, and Ti anomalies in the spidergrams of MG, HG, and LG, which is consistent with the studies of Rollinson (1993). The upper crust has relatively higher Rb/Sr ratios (0.32) as compared with the middle (0.22) and lower (0.04) crust (Rudnick and Fountain 1995). Higher Rb/Sr ratios (0.86–18.70) also reveal emplacement of the MGC magma at the upper crustal level. Depletion of Ba and enrichment of Zr and Y in spidergrams of the MG, HG, and LG reveal a typical pattern of alkaline granites which is analogous to the findings of Oyhantçabal et al. (2007).

Tectonic implications

Geotectonic discrimination diagrams placed MGC plutonic rocks in syn-orogenic, continental-continental collisional fields. Peraluminous, syn-collisional granites commonly occur in regionally metamorphosed areas and are the product of partial melting of metasedimentary rocks (Best 2003; Albarède 2009). Water required for partial melting of source rocks is provided by the breakdown of hydrous minerals like muscovite and biotite (Naeem 2013). The source Tanawal Formation in Mansehra area is composed of mainly pelite-psammite sequence which contains around 8–30% mica contents that formed a potential source for the peraluminous melt of S-type granites of the MGC.

Similar to the convergent regime of Himalaya and Alps (McBirney 2007), the crustal thickening in the zone of convergence in NW Himalaya of Pakistan might have led to the isostatic instability which resulted in the upwelling of deeper crustal material to upper levels. The decompression/extension allowed deeper material to approach towards the surface, brought the heat that induced the low-temperature anatexis in the metasediments of the granite protolith to produce voluminous granitic melt which is analogous to the observations of Gerbi et al. (2006). The isostatic uplift resulted in crustal deformation, thrusting, and extensional regimes provided the space for the emplacement of these granitic bodies. Syn-orogenic deformation squeezed the granitic melt, at the subsolidus stage, towards the down buckled thrust tectogens and emplaced the MGC magma as sheet-like plutonic bodies in the Mansehra area. The presence of myrmekites, undulatory extinctions, marginal mylonization of varied intensity together with microfractured quartz grains, and parallel to the

subparallel alignment of mica flakes suggest crystallization of the granitic melt during the deformational phase, as presented by Pitcher (1993). The occurrence of tectonic foliation, mylonization, and development of local shear zones manifest syn-orogenic subsolidus deformation of the magmatic bodies of the MGC. Partial crustal melting and deformation are synchronous mechanisms that squeezed out the melt to low-pressure areas for emplacement (Sawyer 1994). Segregation and ascent of magma at shallower depth most likely had promoted localized partial melting of the protolith Tanawal Formation and emplaced the magmatic bodies of the MGC. Petrogenesis of early Paleozoic peraluminous S-type granites of Himalaya has generally been related to the compressional regime of the Pan African orogeny at ca. 550–450 Ma (e.g., Sharma and Rashid 2001; Kroner and Stern 2004). Likewise, the genesis of the MGC magmatic rocks was attributed to the Pan African orogeny Le Fort et al. (1983) that was based upon Rb/Sr method. However, Naeem et al. (2016) carried out U-Pb zircon geochronology and assigned ca. 466, 475, and 478 Ma age to the MGC magmatic rocks. In view of the above findings, the Ordovician age has been suggested for the MGC plutonic bodies, and the genesis of these granitic rocks is the result of an Andean-type Cambro-Ordovician event (Bhimphidian orogeny of Cawood et al. 2007) along the eastern margin of Gondwana (Naeem et al. 2016; Ogasawara et al. 2019).

Conclusions

The following conclusions are drawn from this study:

1) The Mansehra Granite is generally massive but occasionally gneissic due to local shearing. The "Susalgali Granite Gneiss" is in fact sheared Mansehra Granite rather than a separate granitic body.
2) Geochemical classification diagrams of the MG, HG, and LG place these granitic bodies in calc-alkaline, peraluminous granitoid fields.
3) The leucogranitic bodies are most likely the product of Na_2O-rich residual melt and boron-rich fluids of the magma crystallizing plutonic bodies of the MGC.
4) The MGC was derived most likely from pelitic metasediments of heterogeneous protolith and is consistent with the peraluminous S-type trait of this Complex. The MGC reveals upper crustal signatures and shallow emplacement (< 15 km).
5) The MG magma was generated most likely by biotite dehydration-melting at > 5 kbr pressure and > 700 °C temperature, while HG melt was formed at relatively shallow levels by localized muscovite fluid-absent melting.
6) The petrogenesis of the MGC plutonic rocks is associated with the Cambro-Ordovician thermo-tectonic episode along the northern margin of east Gondwana.

Acknowledgements We are grateful to Dr. Izhar Ul Haque Khan for analytical facilities and useful discussions. The services of Mr. Zubair Ahmed, Mr. Muhammad Akram, and Mr. Muhammad Sami are thankfully acknowledged for their assistance during field sampling. We are thankful to Mr. Karamat Ali and Mr. Tahir Ali for their help during sample preparation, and Mr. Sami Ullah Khan for thin section preparation. We are thankful to Professor Domenico Doronzo and the anonymous reviewers, for their prolific comments, to improve the quality of the manuscript.

Declarations

Conflict of interest The corresponding author "Dr. Tehseen Zafar" declares that there is no conflict of interest. There is no professional or other personal interest of any nature or kind in any product, service and/or company that could be construed as influencing the manuscript.

References

Albarède F (2009) Geochemistry: an introduction. Cambridge University Press :356
Ashraf M (1992) Petrogenesis of acid minor bodies of Mansehra Granitic Complex, Hazara Himalaya, NW Pakistan. Kashmir J Geol 10:1–26
Batchelor RA, Bowden P (1985) Petrogenetic interpretation of granitoid rock series using multicationic parameters. Chem Geol 48:43–55
Belousova EA, Griffin WL, O'Reilly SY (2006) Zircon crystal morphology, trace elements signatures and Hf isotope composition as a tool for petrogenetic modeling: examples from Eastern Australian granitoids. J Petrol 47:329–353
Best MG (2003) Igneous and metamorphic petrology, second edition. Blackwell Science Ltd:752
Cawood PA, Johnson MRW, Nemchin AA (2007) Early Paleozoic orogenesis along the Indian margin of Gondwana: tectonic response to Gondwana assembly. Earth Plant Lett 255:70–84
Chappell BW, White AJR (2001) Two contrasting granite types: 25 years later. Aust J Earth Sci 48:489–499
Clemens JD, Watkins JM (2001) The fluid regime of high-temperature metamorphism during granitoid magma genesis. Contrib Mineral Petrol 140:600–606
Cox KG, Bell JD, Pankhurst RJ (1979) The interpretation of igneous rocks. George Allen and Unwin, London 450
De La Roche H, Leterrier J, Grandclaude P, Marchal M (1980) A classification of volcanic and plutonic rocks using R1-R2 diagrames and major-element analysis, its relationships with current nomenclature. Chem Geol 29:183–210
Furman NH (1962) Standard methods of chemical analysis. D. Van Nostrand Co., Inc. Princeton, New Jersey
Garcia-Casco A, Haissen F, Castro A, El-Hmidi Torres-Roldan RL, Millan G (2003) Synthesis of staurolite in melting experiments of a natural metapelites: consequences for the phase relations in low-temperature pelitic migmatites. J Petrol 44(10):1727–1757
Gerbi CC, Johnson SE, Koons PO (2006) Controls on low-pressure anatexis. J Metamorph Geol 24:107–118
Hancher JM, Watson EB (2003) Zircon saturation thermometry. In: Hancher, J.M. and Hoskin, P.W.O., (Eds.), zircon. Mineral Soc Am and Geochem Soc Rev in Mineralogy and Geochemistry 53: 89–112
Harris N, Inger S (1992) Trace element modeling of pelite-derived granites. Contrib Mineral Petrol 110:46–56
Harris N, Massey J, Inger S (1993) The role of fluids in the formation of High Himalayan leucogranites. Geol Soc Lond Spec Publ 74:391–400

Hodges KV (2000) Tectonics of the Himalaya and southern Tibet from two perspectives. Geol Soc Am Bull 112:324–350.

Hoskin PW, Schaltegger U (2003) The composition of zircon and igneous and metamorphic petrogenesis. Rev Mineral Geochem 53:27–62

Hoskin PWO, Kinney PD, Wyborn D, Chappell BW (2000) Identifying accessory mineral saturation during differentiation in granitoid magmas: an integral approach. J Petrol 41:1365–1396

Irvin TM, Baragar WR (1971) A guide to the chemical classification of common volcanic rocks. Can J Earth Sci 8:523–548

Janasi VA, Martins L (2003) The Nazare Paulista-type anatectic granite: Mixed sources inferred by elemental geochemistry and Sr-Nd isotopes. Short Papers- IV South American Symposium on Isotope. Geol 572–74

Janousek V, Farrow CM, Erban V (2006) Interpretation of whole-rock geochemical data in igneous geochemistry: introducing Geochemical Data Toolkit (GCDKit). J Petrol 47:1255–1259

Johnson TE, Hudson NFC, Droop GTR (2001) Partial melting of the Inzie Head gneisses The role of water and a petrogenetic grid in KFMASH applicable to anatectic pelitic migmatites. J Metamorph Geol 19:99–118

Jung S, Hoernes S, Masberg P, Hoffer E (1999) The petrogenesis of some migmatites and granites (Central Damara Orogen, Namibia): evidence for disequilibrium melting, wall-rock contamination and crystal fractionation. J Petrol 40:1241–1269

Jung S, Hoernes S, Mezger K (2000) Geochronology and petrogenesis of Pan-African syn-tectonic S-type and post-tectonic A-type granite (Namibia)-products of melting of crustal sources, fractional crystallization and wall-rock contaminant. Lithos 50:259–287

Kerrick DM (1969) K-feldspar-megacrysts from porphyritic monzonite, Central Sierra Nevada, California American Mineralogist. J Earth and Planetary Materials 54:839–843

Khan T, Ahmad A, Rehman HU, Chaudhry MN, Murata M, Zafar M (2019) November. Rb-Sr and Oxygen Isotope Study of the Swat Granite Gneisses (Pakistan): Implications for the Magmatic Source and Tectonic Setup. In Conference of the Arab J Geosci 41–43, Springer, Cham

Kroner A, Stern RJ (2004) Pan African orogeny. Encyclopedia of geology 1 Elsevier, Amsterdam

Le Fort P, Debon F, Sonet J (1980) The "Lesser Himalayan" Cordeirite Granite Belt. Typology and Age of the Pluton of Mansehra (Pakistan). Proc. Intern. Commit. Geodynamics, Grp. 6, Mtg, Peshawar, Nov. 23-29, 179. spec. issue. Geol Bull Univ Peshawar 13:16–61

Le Fort P, Debon F, Sonet J (1983) The Lower Paleozoic "Lesser Himalayan" Granitic Belt: Emphasis on the Simchar Pluton of Central Nepal. In: Shams, F. A., (ed.), Granites of Himalaya, Karakoram and Hindukush:235–255

Maniar PD, Piccoli PM (1989) Tectonic discrimination of granitoids. Geol Soc Am Bull 101:635–643

Mass R, Nicholls IA, Legg C (1997) Igneous and metamorphic enclaves in the Stype Deddick Granodiorite, Lachlan Fold Belt, SE Australia; petrographic, geochemical and Nd-Sr isotopic evidence for crustal melting and magma mixing. J Petrol 38:815–841

McBirney AR (2007) Igneous petrology, 3rd Ed. Jones and Bartlett, publishers, Boston 550

Middlemost EA (1985) An introduction to igneous petrology (magmas and magmatic rocks). Longman, London, New York:266

Middlemost EA (1994) Naming materials in the magma/igneous rock system. Earth Sci Rev 37:215–224

Miller C, Thöni M, Frank W, Grasemann B, Klötzli U, Guntli P, Draganits E (2001) The early Paleozoic magmatic events in the northwest Himalaya, India: source, tectonic setting and age of emplacement. Geol Mag 138:237–251

Miller CF, McDowell SM, Mapes RW (2003) Hot and cold granites? Implication of zircon saturation temperatures and preservations of inheritance. Geology 31:529–532

Mills SJ, Birch WD, Mass R, Philips D, Plimer IR (2008) Lake Boga Granite, northwestern Victoria: mineralogy, geochemistry and geochronology. Aust J Earth Sci 55:281–299

Naeem M (2013) Petrology of Mansehra granitic complex, Hazara area, northwestern Himalaya, Pakistan (doctoral dissertation, University of the Punjab Lahore, Pakistan)

Naeem M, Burg JP, Ahmad N, Chaudhry MN, Khalid P (2016) U-Pb zircon systematics of the Mansehra Granitic Complex: implications on the early Paleozoic orogenesis in NW Himalaya of Pakistan. Geosci J 20:427–447

Nagudi B, Koeberl C, Kurat G (2003) Petrography and geochemistry of the Signo granite, Ugenda, and implications for its origin. J Afr Earth Sci 36:73–87

Norrish K, Hutton JT (1969) An accurate X-ray spectrographic method for the analysis of a wide range of geological samples. Geochim Cosmochim Acta 33:431–453

Ogasawara M, Fukuyama M, Siddiqui RH, Zhao Y (2019) Origin of the Ordovician Mansehra granite in the NW Himalaya, Pakistan: constraints from Sr–Nd isotopic data, zircon U–Pb age and Hf isotopes. Geol Soc London Spec Publ 481:277–298

Oyhantçabal P, Siegesmund S, Wemmer K, Frei R, Layer P (2007) Post-collisional transition from calc-alkaline to alkaline magmatism during transcurrent deformation in the southernmost Dom Feliciano Belt (Braziliano-Pan-African, Uruguay). Lithos 98:141–159

Pant NC, Kundu A (2008) Geochemical characters of muscovite from the Pan African Mandi Granite, and its emplacement and evolution. Himal J Sci 5:98

Patino-Douce AE, Johnston AD (1991) Phase equilibria and melt productivity in the pelite system: implications for the origin of peraluminous granitoids and aluminous granulites. Contrib Mineral Petrol 107:202–218

Pickering JM, Johnston AD (1998) Fluid-absent melting behaviour of a two-mica metapelites; Experimental constraints on the origin of Black Hill granite. J Petrol 39:1787–1804

Pitcher WS (1993) The nature and origin of granitic rocks. Chapman and Hall, Glasgow 321

Regmi KR (2008) Petrogenesis of the augen gneisses from Mahesh Kola section, Central Nepal. Bull Dep Geol 11:13–22

Rollinson H (1993) Using Geochemical Data: Evaluation, Presentation and Interpretation. Longman, Harlow:352

Rudnick RL, Fountain DM (1995) Nature and composition of the continental crust: a lower crustal perspective. Rev Geophys 33:267–309

Sawyer EW (1994) Melt segregation in the continental crust. Geology 22: 1019–1022

Shams FA (1971) The geology of the Mansehra-Amb State area, Northern West Pakistan. Geol Bull Univ Punjabb, Lahore 8:1–31

Shams FA, Rehman FU (1967) An estimation of temperature of formation of some granitic rocks of the Mansehra-Amb State area, Northern west Pakistan, and its bearing on their petrogenesis. Geol Bull Punjab Univ Lahore 6:39–43

Shand SJ (1943) Eruptive rocks: their genesis, composition, and classification, with a chapter on meteorites. J Wiley & sons Incorporated New York: 444

Sharma KK, Rashid SA (2001) Geochemical evolution of peraluminous paleoproterozoic Bandal Orthogneiss NW Himalaya, Himachal Predesh, India: implications for the ancient crustal growth in the Himalaya. J Asian Earth Sci 19:413–428

Singh RKB (2010) Geochemistry and petrogenesis of granitoids of Lesser Himalayan crystallines, Western Arunchal Himalaya. J Geol Soc India 75:618–631

Singh S, Jain AK (2003) Himalayan granitoids. J Virtual Explor 11:1–20

Singh B, Kumar S (2005) Petrogenetic appraisal of early Paleozoic granitoids of Kinnaur district, Higher Himachal Himalaya, India. Gondwana Res 8:67–76

Sylvester PJ (1998) Post-collisional strongly peraluminous granites. Lithos 45:29–44

Vielzeuf D, Schmidt MW (2001) Melting relations in hydrous systems revisited: application to metapelites, metagreywackes and metabasalts. Contrib Mineral Petrol 141:251–267

Villaros A, Sevens G, Moyen JF, Buick IS (2009) The trace element compositions of S-type granites: evidence for disequilibrium melting and accessory phase entrainment in the source. Contrib Mineral Petrol 158:543–561

Watson EB, Harrison TM (1983) Zircon saturation revisited; temperature and composition effects in a variety of crustal magma types. Earth Planet Sci Lett 64:295–304

Yurimoto H, Duke EF, Peipike JJ, Shearer CK (1990) Are discontinuous chondrite-normalized REE pattern in pegmatitic granite systems the result of monazite fractionation? Geochim Cosmochim Acta 54: 2141–2145

Zafar T, Mahar MA, Rehman HU, Riaz M, Latif K, Oyebamiji A, Naeem M (2019) Geochemical and petrological characteristics of xenoliths in Mansehra Granite, NW Himalaya, Pakistan: implications for petrogenesis and tectonic settings. Episodes J Intern Geoscience 42: 263–285